Chapter 4

Hyperspectral Imaging for Assessing Quality and Safety of Meat

Wenxiu Wang and Yankun Peng

Additional information is available at the end of the chapter

http://dx.doi.org/10.5772/intechopen.74371

Abstract

Hyperspectral imaging (HSI) technology is a novel nondestructive method and has found various applications in the agricultural and food industry. In this chapter, the employment of HSI for meat quality assessment and safety control was summarized. The quality attributes include sensory attributes (color and marbling), chemical attributes (moisture, protein, intramuscular fat, and fatty acids), and technological attributes (pH, tenderness, and water holding capacity (WHC)). The safety attributes mainly include bacterial contamination and freshness determination. The spectral method is described in terms of the basic working principle, fundamental configurations, analysis period, and applications in meat assessment. In addition, the advantages, disadvantages, and problems to be tackled facing the HSI are also discussed. The current studies have demonstrated that HSI technology can be a potential tool to replace the traditional method for online and simultaneous evaluation of multiple quality and safety attributes of meat.

Keywords: hyperspectral imaging, meat, quality, safety, nondestructive detection

1. Introduction

Meat is an important element in human's diet as it is rich in easily digestible protein, vitamins, minerals, and micronutrients [1]. The improvement of living standards has prompted people to pay more attention to quality and safety, which are two crucial aspects related with meat. Quality refers to a comprehensive property about the sensory, chemical, and technological attributes of meat. The sensory attributes, such as color and marbling scores (MS), are about the first expression on meat and will influence consumers' willingness to purchase. Chemical attributes include moisture, protein, intramuscular fat (IMF), fatty acids (FAs), etc., and they

are concerned with nutritive value and human health. Technological attributes like pH, water holding capacity (WHC), and tenderness are important factors that affect the eating quality [2]. Safety is another concern about meat, which can be challenged in several ways, such as biological issues and chemical contamination [3]. The former is considered as the biggest threat. This is because meat is ease of perishability and is suitable for the microbial growth.

The conventional methods for determination of the aforementioned traits include sensory evaluation and instrumental analysis [4]. They can provide accurate results and have been used for decades. However, they have some drawbacks as they are destructive, time-consuming, and labor-intensive. To match up with the demands of producers, manufacturers, distributors, retailers, and especially consumers for reliable and real-time evaluation of meat, nondestructive, rapid, and efficient tools are in urgent need. Hyperspectral imaging (HSI) technology has emerged as an alternative method. It combines the advantages of spectroscopic and imaging techniques and can acquire the spatial and spectral information simultaneously [5]. Owing to the merits, it has found numerous applications in agro-products for determination of internal traits and external features [6, 7]. A typical hyperspectral reflectance measurement system is shown in **Figure 1**, which mainly consists of a CCD camera, an imaging spectrograph, a zoom lens, illumination, computer, etc. When obtaining scattering images, an optical fiber is usually needed to form a point light source [8]. The hyperspectral data are collected in a three-dimensional (3D) form called "hypercube," among which two dimensions are spatial information expressed in x and y, and the third dimension is wavelength information, which is represented with λ [9].

After acquisition of reflectance images, chemometric tools are required to relate them and reference values of tested samples. Generally, the image is corrected and segmented first. Then, a range of interest (ROI) is selected and the mean spectrum is extracted from it. **Figure 2** shows the reflectance spectra extracted from a pixel. Subsequently, the spectrum undergoes (1) pretreatments to reduce and correct the adverse interferences caused by scattering, baseline drift, etc. The commonly used methods include Savitzky-Golay (SG)

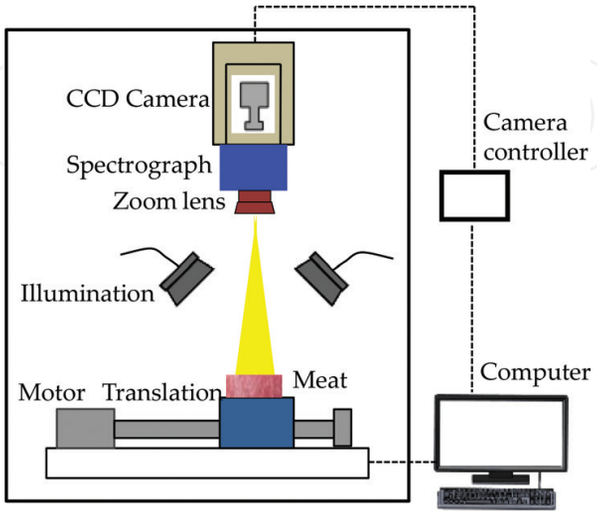

Figure 1. Schematic diagram of a hyperspectral reflectance measurement system.

http://dx.doi.org/10.5772/intechopen.74371

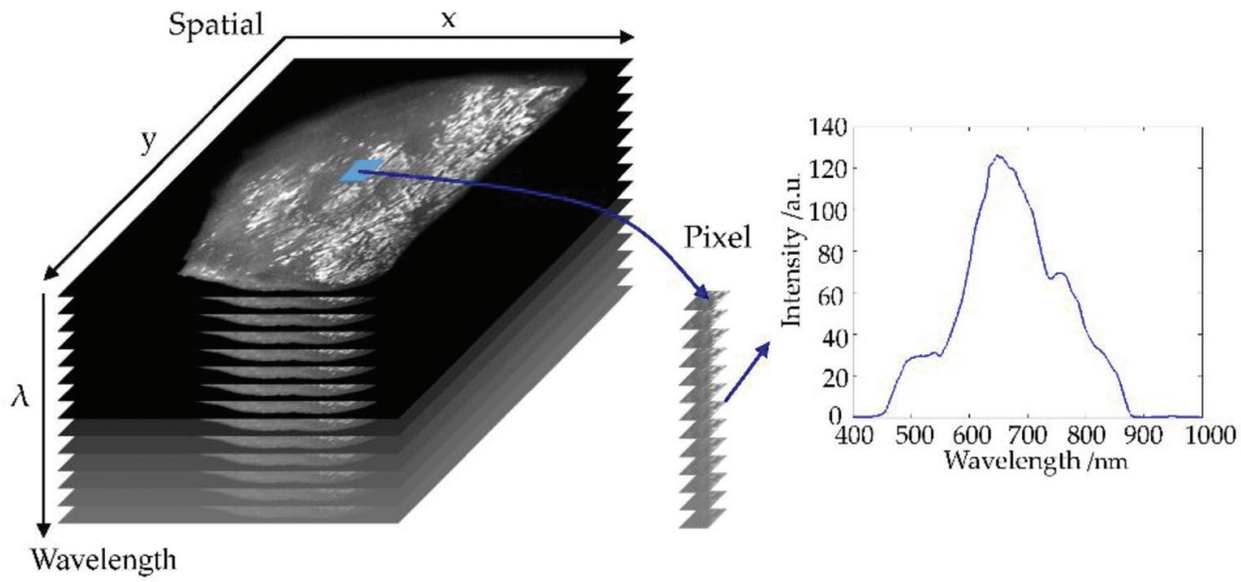

Figure 2. Reflectance spectra extracted from hyperspectral image.

smoothing, derivation, standard normal variate transformation (SNVT), orthogonal signal correction (OSC), and so on [10]; (2) feature wavelengths selection to eliminate the unwanted information and retain the characteristic wavelengths for simplifying the modeling. Genetic algorithm (GA), successive projection algorithm (SPA), uninformative variable elimination (UVE), etc. are efficient approaches for this purpose; (3) model establishment for quantitative or qualitative analysis using partial least squares regression (PLSR), multiple linear regression (MLR), least squares support vector machine (LS-SVM), and so on. In this case, chemical maps can be created by transferring the model to every pixel in the image to show distributions of each ingredient in a pixel-wise manner. Usually, the models are evaluated with correlation coefficient of calibration, prediction, and cross validation (R_c, R_p, and R_{cv}) and coefficient of determination for the calibration, prediction, and cross validation (R_c^2, R_p^2, and R_{cv}^2).

As to the spatially resolved hyperspectral images, effective nonlinear curve-fitting algorithms are usually required to extract scattering characteristics. Lorentzian distribution function is one of them, which has been intensively used in optic research to describe the light distribution patterns. It has three forms of expression: two-parameter, three-parameter, and four-parameter [11], and they are expressed as shown in Eqs. (1)–(3):

$$R = \frac{b}{1+(x/c)^2} \tag{1}$$

$$R = a + \frac{b}{1+(x/c)^2} \tag{2}$$

$$R = a + \frac{b}{1+(x/c)^d} \tag{3}$$

where R represents the light intensity, x is the scattering distance, a is the asymptotic value, b represents the peak value, c is the full width at $b/2$, and d is the slope around the inflection point. Similar with the Lorentzian distribution function, Gompertz function also has three forms of expression, namely, two-parameter, three-parameter, and four-parameter functions [11]. Eqs. (4)–(6) show their mathematical expressions:

$$R = 1 - \exp\{\exp(\varepsilon - \delta x)\} \tag{4}$$

$$R = 1 - (1 - \alpha)\exp\{-\exp(\varepsilon - \delta x)\} \tag{5}$$

$$R = \alpha + \beta\left[1 - \exp\{-\exp(\varepsilon - \delta x)\}\right] \tag{6}$$

where R represents the light intensity, x is the scattering distance, α is the asymptotic value, β is the upper value, ε represents the full scattering width, and δ is the slope value. Boltzmann function is another equation to describe light scattering and absorption in turbid materials. Absorption coefficient (μ_a) and scattering coefficient (μ_s') can be extracted to characterize the chemical or physical properties of tested samples. A more detailed introduction to the fitting functions was given by Peng [12].

As a vast number of data are contained in a hyperspectral image, the high-dimensional nature increases the difficulty in acquiring and processing the huge data. Multispectral imaging (MSI) is a simplified version, which uses few (generally less than 10) discrete spectral images. By acquiring the spatial and spectral information that are directly useful for meat detection, the experiment and analysis period are simplified [13]. Besides, simpler algorithms are needed, and the data size is decreased significantly, making it feasible to be implemented in the field or industry for real-time applications.

2. Quality assessment using HSI

2.1. Sensory quality attributes

Of all the sensory attributes, color is one of the most critical indicators which determine the first impression on meat for consumers. Meanwhile, they also reflect the freshness degree of meat and will in turn affect consumers' willingness to purchase. Color is related with the content and molecular type of myoglobin and hemoglobin in meat. Conventionally, the meat color is measured by means of a colorimeter to obtain the L^* (light), a^* (red-green), and b^* (yellow-blue). Marbling pattern is another important indicator, which would directly influence the grade and price of meat. The grading of meat is commonly conducted by well-trained professionals referring to different carcass grading standards.

To overcome the shortcomings of subjectivity and laboriousness in the traditional method, a HSI system in the spectral range of 400–1100 nm (**Figure 3a**) was used to acquire the scattering

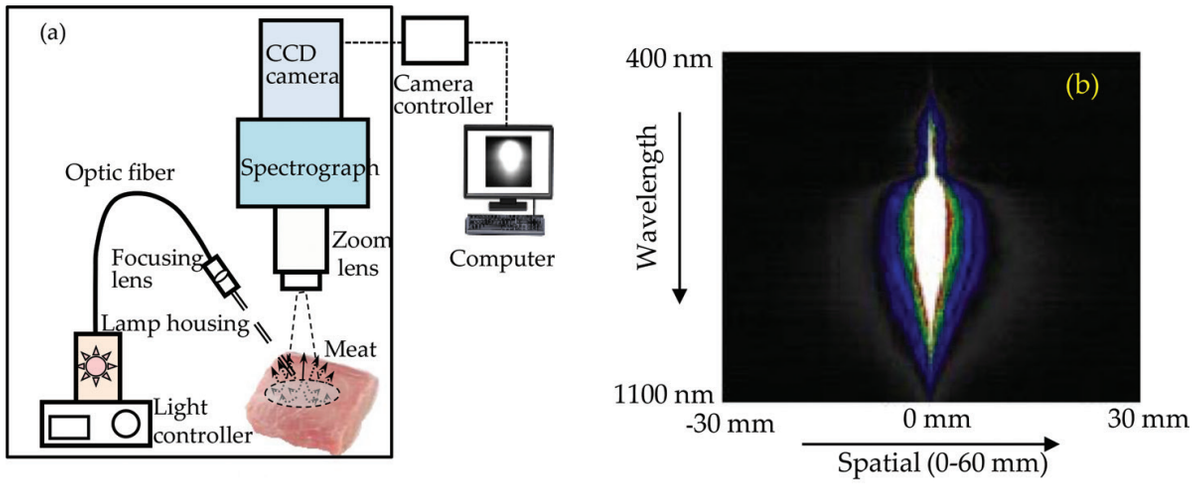

Figure 3. (a) Acquisition system for hyperspectral scattering image and (b) original scattering image for beef sample.

images of beef samples [14]. Different from that in **Figure 1**, a halogen tungsten lamp coupled with an optical fiber constituted the light source unit. The hyperspectral image was shown in **Figure 3b**, in which the vertical axis was wavelength axis and the horizontal axis represented the spatial distance. Then, three-parameter Lorentzian distribution function was employed to fit the scattering profile. A good fitting effect was observed between 450 and 1090 nm with the correlation coefficient greater than 0.90. The wavelengths below 450 nm and above 1090 nm contained considerable noise; hence, they were eliminated in the subsequent analysis.

Stepwise regression analysis was performed to determine the characteristic wavelengths before model establishment. Seven, seven, and eight wavelengths were selected for L^*, a^*, and b^*, respectively, as shown in **Table 1**. Most of the identified wavelengths were related with deoxymyoglobin, oxymyoglobin, metmyoglobin, and sulfmyoglobin. Then, MLR models based on the combined Lorentzian parameters were created with R_{cv} of 0.96, 0.96, and 0.97 for L^*, a^*, and b^*, respectively. The satisfactory results demonstrated the feasibility of spatially scattering information for color evaluation.

The nondestructive determination of meat color based on reflectance spectra was also carried out. Hyperspectral images of beef, lamb, and pork in the range of 400–1000 nm were collected [15]. Unlike the previous studies in which different feature wavelengths were selected for each attribute, a set of important variables were identified for L^*, a^*, and b^* to create models. They were 450, 460, 600, 620, 820, and 980 nm, which had little deviation from those chosen in

Quality attributes	Feature wavelengths (nm)
L^*	653, 678, 722, 868, 875, 920, 1050
a^*	465, 575, 614, 635, 671, 724, 978
b^*	486, 524, 540, 645, 700, 721, 780, 954

Table 1. Feature wavelengths for color selected by stepwise regression analysis.

Ref. [14]. The differences in image acquisition system and chemical compositions of meat may account for the deviation. Based on the six wavelengths, MLR models were built which gave R_p^2 of 0.97, 0.84, and 0.82 for L^*, a^*, and b^*. The results also laid foundation for the development of MSI detection device for color determination.

The capacity of HSI technology for beef marbling grade analysis has been confirmed. Images of a total of 33 beef samples were collected and divided into seven grades, 1, 1.5, 2, 2.5, 3, 3.5, and 4, according to the industry standard NY/T 676–2003 [16]. **Figure 4** showed the image of a sample with grade of 3 at 470, 550, 600, 660, 720, 850, and 950 nm. The eighth one in **Figure 4** was the combination of images at 720 (red), 550 (green), and 470 nm (blue). It can be seen that higher brightness and stronger muscle reflexes were found in the near-infrared region. In the visible region, the muscles and fat had larger contrast, which was favorable for marbling segmentation. Then, ROIs for the muscle and fat were selected, respectively, and their mean reflectance spectra were extracted from the ROI. Calculate the reflection intensity ratios of the muscle and fat at each wavelength, and the biggest ratio was observed at 530 nm. Hence, it was identified as the optimal wavelength for marbling feature extraction.

Based on the images at 530 nm, big fat area (higher than 14.88 mm^2 which corresponded to 75 pixels), medium fat area (between 3.72 and 14.88 mm^2), and small fat area (below 3.72 mm^2 which corresponded to 20 pixels) were calculated. Taking the three parameters as independent variables, MLR model was built with R_{cv}^2 of 0.92 and standard error of cross validation (SECV) of 0.45. Meanwhile, the regular decision function was also trialed to relate the image features and marbling grades with classification accuracy of 78.8%, which was lower than MLR model (84.8%). The overall results were satisfactory and demonstrated the feasibility of HSI for marbling evaluation.

The marbling scores of fresh, frozen, and frozen-thawed pork were quantified by a HSI system in the range of 900–1700 nm [17]. After ROI selection, a Gabor filter was performed

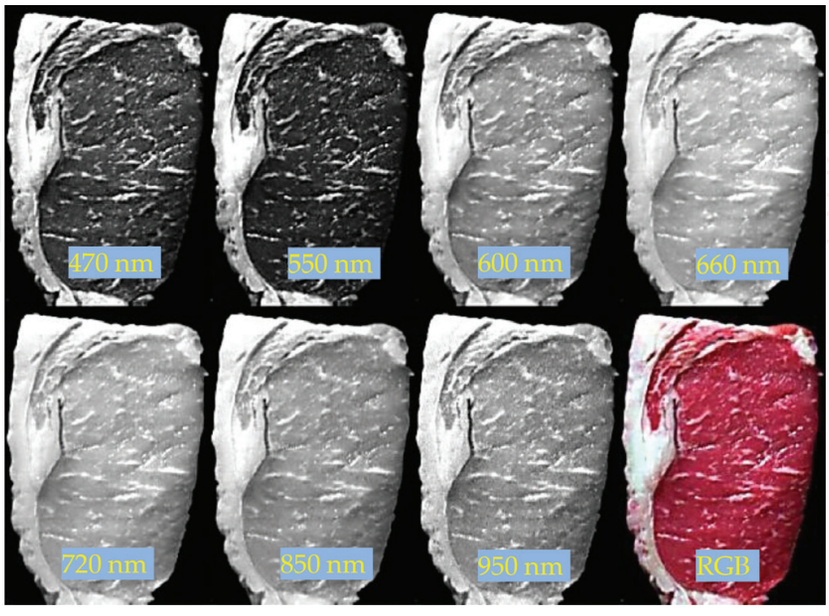

Figure 4. Images at seven wavelengths and RGB image of beef sample.

Sample	Image features	Key wavelengths	R_c	R_{cv}	R_p
Fresh	DMR	1082, 1188, 1217, 1236, 1452	0.85	0.83	0.91
Fresh	DMG	1082, 1188, 1236, 1346, 1380	0.88	0.86	0.88
Frozen	DMR	1217, 1236	0.84	0.83	0.90
Frozen	DMG	1217, 1231, 1264, 1514	0.83	0.83	0.85
Frozen-thawed	DMR	1169, 1255	0.82	0.81	0.89
Frozen-thawed	DMG	1078, 1174, 1226, 1346, 1433	0.89	0.87	0.91

Note: DMR and DMG represented the first derivative spectra of raw and Gabor-filtered images. R_c, R_{cv}, and R_p represented the correlation coefficient of calibration, cross validation, and prediction, respectively.

Table 2. Selected key wavelengths and model performance.

on the images, and the mean Gabor-filtered spectra and raw spectra were obtained. Then, they were pretreated with first derivative (FD), and MLR models were built linking the processed spectra at the feature wavelengths and marbling scores. The wavelengths selected and model results for fresh, frozen, and frozen-thawed pork were shown in **Table 2**. The promising results confirmed the capacity of Gabor filter technique in extracting image features.

2.2. Chemical quality attributes

Of all the chemical compositions, moisture, protein, and IMF are three major components of meat. FAs are also important indicators and have attracted more and more attentions in recent days. The reasons may be that the amount and types of FAs would influence other attributes and they also had some relationship with the cardiovascular diseases [18]. The traditional measurement methods for those attributes were drying method, Soxhlet method, Kjeldahl method, or gas chromatographic method. They are destructive, time-consuming, and laborious and cannot realize simultaneous detection of multiple attributes. As these chemical compositions contained C—H, N—H, or O—H bonds, the applications of HSI mainly focused on the usage of reflectance spectra to realize nondestructive determination.

A HSI system in the range of 900–1700 nm was used for determination of moisture, IMF, and protein in lamb meat [19]. A total of 126 samples containing three different muscles (semitendinosus (ST), semimembranosus (SM), and longissimus dorsi (LD)) were employed for hyperspectral image acquisition and reference analysis. After image correction and segmentation, spectral data were extracted from the ROIs. Samples were divided into calibration and validation set according to a ratio of 2:1, namely, 84 *vs*. 42 samples. The ranges of moisture, IMF, and protein in the calibration set were 69.65–76.35, 0.75–7.62, and 21.30–24.05%. In the prediction set, the ranges were 69.45–75.64, 0.74–6.01, and 21.24–23.84%. The moisture and IMF had a big standard deviation, while the protein had a relatively small standard deviation.

First, PLSR models based on full-band spectra were built. R_{cv}^2 of 0.94, 0.94, and 0.67 were found for moisture, IMF, and protein. The reason for the poor prediction ability for protein may be

the narrow range of reference. To enhance the model for protein, some samples were minced with adjoined fat portion of the muscle to increase the reference ranges to 16.30–24.05%. New PLSR model was then built based on the modified data with R_{cv}^2 of 0.85, indicating a significant improvement. Feature wavelengths were further selected according to the regression coefficients obtained from the PLSR models. For moisture and IMF, 6 out of 237 wavelengths were selected, namely, 960, 1057, 1131, 1211, 1308, and 1394 nm. For protein, 1008, 1211, 1315, 1445, 1562, and 1649 nm were identified as the important wavelengths. Simplified models were again created with R_{cv}^2 of 0.86, 0.90, and 0.83 for moisture, IMF, and protein. The results were similar with those using the whole spectral range, which confirmed the capacity of HSI for prediction of chemical compositions.

As to the FA prediction using HSI, few studies were conducted. A HSI system in the near-infrared range of 1000–2300 nm was used to detect the FAs in intact raw beef cuts [20]. The FAs included the total saturated fatty acid (SFA), total unsaturated fatty acid (UFA), myristic (C14:0), palmitic (C16:0), stearic (C18:0), myristoleic (C14:1), palmitoleic (C16:1), oleic (C18:1), and linoleic (C18:2) acids. Similar with the aforementioned procedure, reflectance spectra were extracted and converted to absorbance values. Multiple scattering correction (MSC) was conducted on the absorbance spectra to correct spectral intensity differences. PLSR models were then built, yielding satisfactory results for SFA and UFA with R_p^2 of 0.87 and 0.89. For other attributes, the R_p^2 varied from 0.68 to 0.89. Apply the models to every pixel in the hyperspectral images, the chemical maps were generated, and the distributions of each composition can be observed intuitively.

2.3. Technological quality attributes

The technological quality attributes of meat mainly include pH, tenderness, and WHC, which are related to some structural and biochemical phenomena in living or carcass muscles. These attributes depend not only on the type of animal feed and fatty acid composition of carcass but also on the maturation effect. pH is considered as an important indicator of meat quality as it affects the color, tenderness, flavor after cooking, shelf life, and water retention. Meanwhile, it is also a reference to judge the meat freshness as it increases when meat turns spoiled. The traditional measurement for pH is by means of a pH meter to insert it into the meat. Tenderness directly affects the eating quality and commodity value of meat. It is closely related with the muscle structure (connective tissue) and biochemical composition (proteolysis of myofibrils and cytoskeletal proteins) of meat. Sensory evaluation and Warner-Bratzler shear force (WBSF) or slice shear force (SSF) are currently used methods for tenderness determination. WHC refers to the ability of the muscle to retain water and is an important factor that affects the color, flavor, and tenderness of meat. The conventional measurement methods include cooking loss method, drip loss method, squeezing method, and so on.

The determination of technological attributes using hyperspectral scattering imaging technique had been explored, and satisfactory results were obtained. Similar with the aforementioned analysis procedure for color, predictive models were built to relate the multiple "parameter spectra" of Lorentzian, Gompertz, or Boltzmann function and reference values. A sample of this topic about tenderness evaluation was given in Ref. [21]. A total of 31 pork

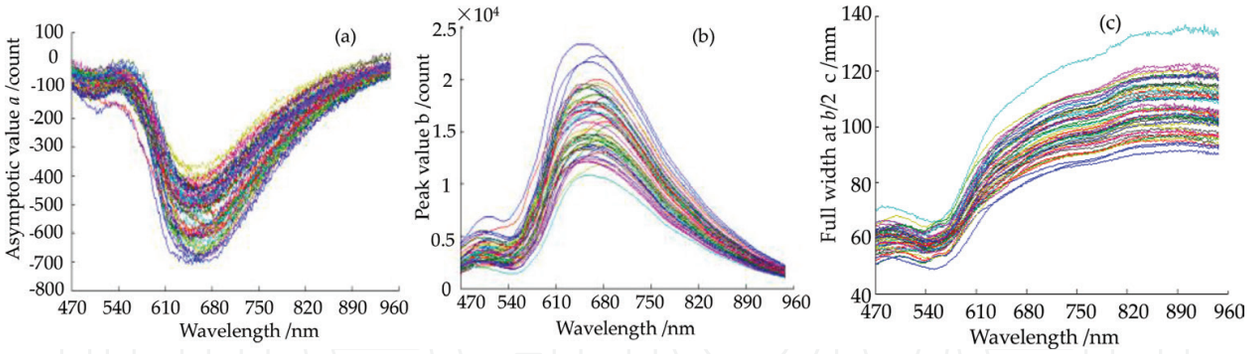

Figure 5. Lorentzian parameters extracted from pork images: (a) parameter *a,* (b) parameter *b*, and (c) parameter *c*.

samples were collected for scattering image acquisition and tenderness measurement by WBSF method. Then, the authors used three-parameter Lorentzian distribution function to fit the scattering profile, and accurate fitting performance was observed. For example, the fitting correlation coefficient at 575 nm was 0.998. Individual parameters *a*, *b*, and *c* (as shown in **Figure 5**) and the combination parameters of (*b*-*a*), (*b*-*a*) × *c*, (*b*-*a*)/*c,* and "*a*&*b*&*c*" were extracted. Likewise, stepwise regression analysis was performed to determine the optimal wavelength combinations for each parameter. Comparison of results showed that the models based on parameters *a*, *b*, (*b*-*a*), and (*b*-*a*)/*c* performed better with R_{cv} of 0.831, 0.860, 0.856, and 0.930, respectively.

Meanwhile, the modified Gompertz function was also employed to extract scattering characteristic of pork samples [22]. Promising fitting performance was found between 470 and 960 nm with coefficients all around 0.99. Parameters α, β, ε, and δ were then extracted, and their spectra at each wavelength were shown in **Figure 6**. As no optimal wavelengths were found for parameter β, hence, MLR models based on individual (α, ε, and δ) and integrated (α&ε&δ) were established and compared. The model based on the integrated one was superior to others with R_{cv} of 0.949, due to that more comprehensive information was involved. The overall results were better than the best result using Lorentzian parameter (*b*-*a*)/*c* (R_{cv} = 0.930).

Studies on using reflectance spectra in conjunction with multivariate analysis for noncontact measurement of pH, tenderness, and WHC have been conducted intensively. Hyperspectral images in the range of 900–1700 nm of beef samples were collected to predict WHC [23]. Samples were prepared with three different breeds and different muscles (*M. longissimus* dorsi (LD), M. semitendinosus (ST), and Psoas major (PM)). Thus, the reference values of WHC had a large variation, which was beneficial to build a robust model. PLSR model was then built to correlate the spectra and reference values measured by drip loss method, and an R_{cv}^2 of 0.89 was obtained. According to the regression coefficients of PLSR model, six important wavelengths at the peak positions were further selected, namely, 940, 997, 1144, 1214, 1342, and 1443 nm. New PLSR model based on the feature wavelengths was created with R_{cv}^2 of 0.87, demonstrating the potential of HSI for postmortem nondestructive determination of WHC. Key wavelengths for WHC in lamb meat in the range of 400–1000 nm were identified as 545, 610, 705, 765, 805, 900, 940, and 970 nm in Ref. [24]. Based on these wavelengths, LS-SVM model was built, yielding a good prediction performance with R_p^2 of 0.93.

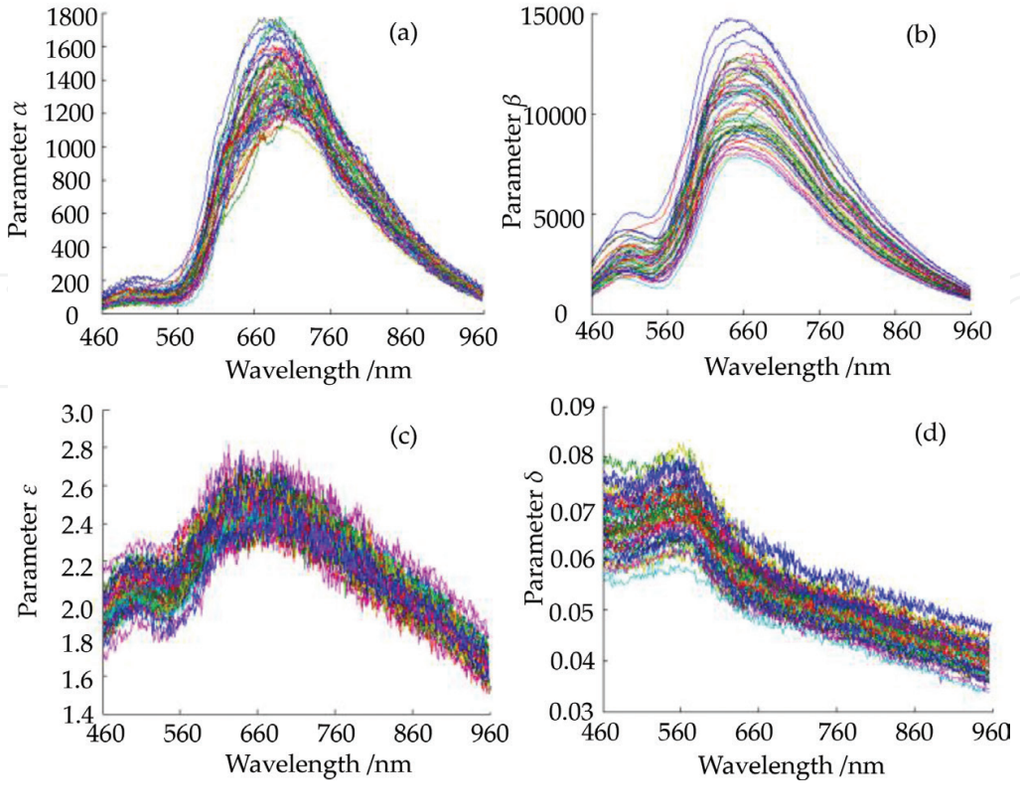

Figure 6. Gompertz parameters extracted from pork samples: (a) parameter α, (b) parameter β, (c) parameter ε, and (d) parameter δ.

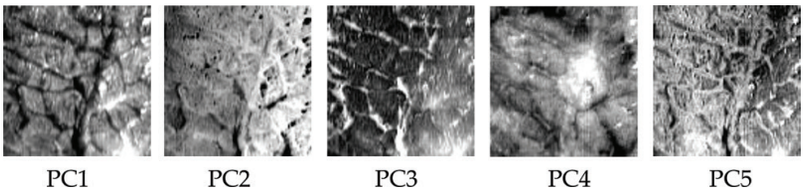

Figure 7. PC1–PC5 feature images for beef sample.

Besides, the feasibility of texture feature in predicting beef tenderness was also explored [25]. Three hundred and ninety-four hyperspectral images between 480 and 1020 nm were selected for each beef sample. Principal component analysis (PCA) was first conducted on these images to reduce the data dimension. The first five principal component images (PC1–PC5) are shown in **Figure 7**. It can be seen that the PC1 image contained most of the original image information with contribution rate more than 85%. The PC2 image contained little efficient information, while the PC3 image provided complementary information to PC1. The variance contribution rate of the first three principal component images was 95.37%, which was enough to represent the original information of the sample.

Further, gray-level co-occurrence matrix (GLCM) was used to extract texture variables from the three PCA images. Eight characteristic parameters including the mean, contrast, entropy,

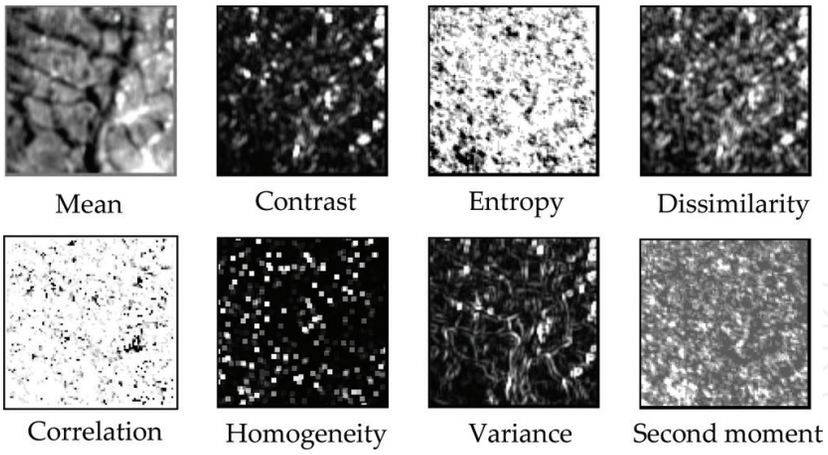

Figure 8. Eight texture features for image at 630 nm.

dissimilarity, correlation, homogeneity, variance, and second moment were obtained. **Figure 8** showed the texture features for the image at 630 nm. Thus, a total of 24 features were acquired for each sample. Taking them as the input variables, SVM and linear discrimination analysis (LDA) were established. The comparison of classification model results showed that LDA model had better performance than SVM with accuracy in the prediction set of 94.44%. The study also indicated that texture features can be used to determine the distribution of meat tenderness.

3. Safety control using HSI

Meat safety refers to the potential threat to human health. The applications of HSI on safety control mainly focused on the bacterial contamination and freshness determination. Bacterial contamination, often expressed as total viable counts (TVC), is an important microbiological indicator to determine the contamination and spoilage degree of meat. It is also used to predict the shelf life of meat or meat products. The quantity of 10^6 colony-forming units per gram (CFU/g) is considered as an acceptable limit, beyond which the meat became inedible [26]. Pseudomonas is a specific spoilage bacteria for meat stored at 4°C. The present method to evaluate TVC is plate-counting method, which is cumbersome and time-consuming and cannot satisfy the requirement for real-time detection. Freshness is a combination of flavor, taste, color, texture, and taste, and it is also a critical criterion to measure whether the meat meets the consumption standard. During the storage, proteins in meat tissue are broken down into low-molecular metabolites (alkaline substances such as ammonia and amines) with the action of enzymes and bacteria. Then, they are combined with acid within meat and form total volatile basic nitrogen (TVB-N) [27]. Traditional methods available for TVB-N detection include semimicro nitrogen determination and micro-diffusion method. They are time-consuming and destructive; hence, rapid and noncontact analytical methods are encouraged for TVB-N detection.

3.1. Bacterial contamination detection using HSI

In the previous studies, the ability of spatially scattering images for TVC, *Escherichia coli*, and Pseudomonas determination has been demonstrated. Such examples were given in Refs. [21, 28–29]. Hyperspectral images of beef samples stored within 2 weeks were collected [30]. To increase the signal-to-noise ratio of images, a 2 × 2 union (binning) operation was conducted, and then images of 520 × 688 pixels were acquired. For each sample, 4 different positions were selected for scanning and 4 times per position; thus, a total of 16 images were acquired for each sample. The reference values for TVC was then measured and recorded as $\log_{10}$CFU/g. **Figure 9** showed the bacterial growth curves. It can be seen that with storage time passed by, the TVC increased from 4.89 to 8.89.

Then, two-parameter Lorentzian distribution function was used to fit the scattering profiles. Parameters b, c, and $b \times c$ were obtained, and their correlation coefficients with $\log_{10}$CFU/g were shown in **Figure 10**. A similar trend was observed for the three parameters, especially for parameters b and $b \times c$, which had almost the same correlation coefficients over the range of 560–770 nm. Stepwise regression analysis was further performed to select the representative wavelengths for each parameter, as shown in **Table 3**. MLR models were established based on these wavelengths, and the results were also shown in **Table 3**. It can be seen that parameter $b \times c$ performed the best with R_p^2 of 0.96 and standard error of prediction set (SEP) of 0.23. The results demonstrated the feasibility of HSI for nondestructive determination of TVC.

The potential of reflectance spectra for bacterial contamination measurement has also been explored, and satisfactory results were obtained. Zheng et al. conducted a study to build a precise and simple model with low cost for TVC of pork [31]. Fifty chilled pork samples were collected and stored in a refrigerator at 4°C. Hyperspectral images in the range of 400–1100 nm were acquired, and spectra were extracted from a ROI and averaged. The original spectra for all the experimental samples were shown in **Figure 11**. Crests and troughs were observed between 530 and 580 nm, which were reported to be associated with myoglobin. The absorption peak at 980 nm was related to water absorption, corresponding to the second overtones of O—H stretching.

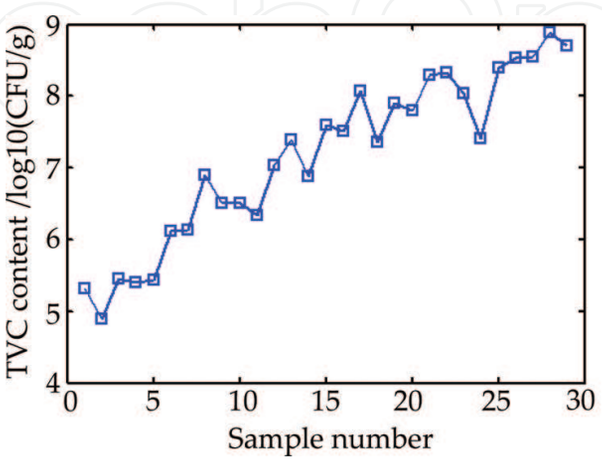

Figure 9. Bacterial growth curves during storage.

http://dx.doi.org/10.5772/intechopen.74371

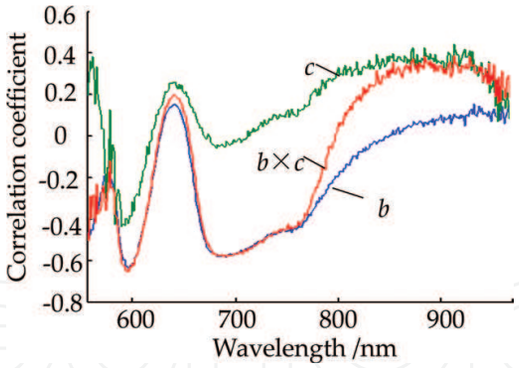

Figure 10. Correlation coefficients of parameters *b*, *c*, and *b* × *c* with $\log_{10}$CFU/g.

Parameter	Feature wavelengths (nm)	SEC	SEP	R_p^2	RSD (%)
b	592, 596, 602, 659, 803, 825	0.48	0.47	0.91	6.30
c	596, 838, 905, 913	0.70	0.62	0.69	8.31
b × *c*	596, 822, 838, 841, 889, 900	0.44	0.23	0.96	3.08

Note: SEC, standard error of calibration set; SEP, standard error of prediction set; R_p^2, determination coefficient in the prediction set; RSD, relative standard deviation.

Table 3. Selected feature wavelengths and modeling results.

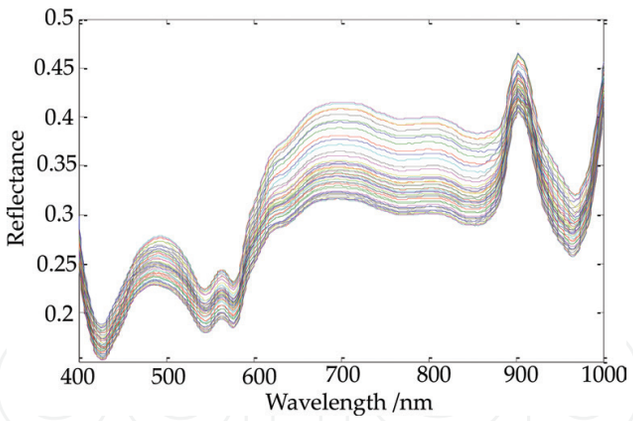

Figure 11. Original reflectance spectra of 50 pork samples.

To improve model accuracy, different pretreatment methods including SNVT, MSC, FD, second derivative (2D), Haar transformation (HT), and centering transformation (CT) were tried. Linear and nonlinear models, namely, PLSR and support vector regression (SVR) models, were built and compared. The SVR model combined with 2D pretreatment yielded the best result, with R_c and R_p of 0.99 and 0.94. Applying the optimal model to the hyperspectral images, the spatial distribution of bacteria can be observed clearly. **Figure 12** showed the chemical maps of TVC at different contamination levels, and the prediction results can be observed intuitively. It can be seen that there was an evident tendency of color change with

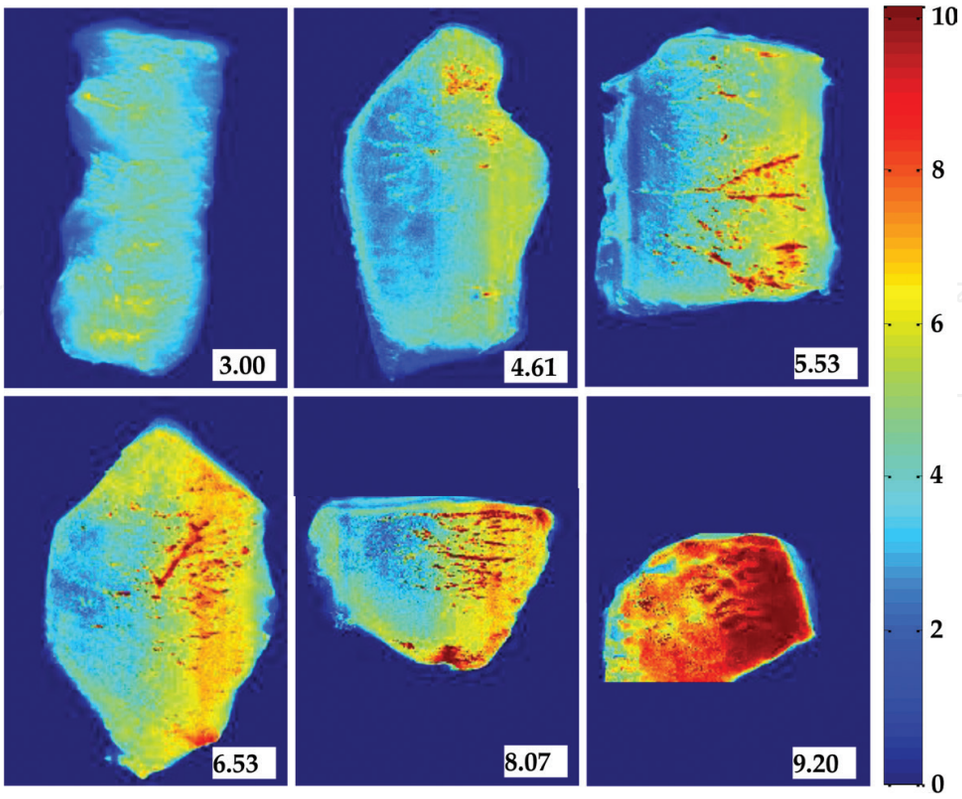

Figure 12. Visualizing maps of pork samples with different TVC values.

the increase of TVC content. When the bacterial contamination level was low, the density of blue color was dominant. In contrast, the red color occupied almost the whole image when the TVC content was 9.20. The change in color was inconsistent with the microbial content, which verified the prediction capacity of HSI for real-time monitoring of the bacterial contamination level.

In addition to these studies using HSI to predict TVC, MSI also demonstrated the application potential for TVC determination. One example was given in Ref. [32]. The authors used a rapid MSI device to detect pork spoilage with different storage temperatures (0, 5, 10, 15, and 20°C) and package types (aerobic and modified atmosphere). A reasonable prediction result for TVC was obtained with SEP of 7.47%, demonstrating the feasibility of using the setup to predict microbial counts in minced meat. Study for beef detection was carried out in Ref. [33]. The authors explored the capacity of MSI in determining microbial counts of aerobically packaged beef stored at different temperatures (0, 4, 8, 12, and 16°C). Average estimation deviations of 11.6, 13.6, and 16.7% were obtained for *Pseudomonas* spp., *B. thermosphacta*, and TVC, respectively. In recent days, "signature" spectra of contaminated aerobically packaged beef stored at 2, 8, and 15°C were extracted using MSI technique in Ref. [34]. According to a threshold of 2 $\log_{10}$CFU/g, samples were discriminated into two classes with accuracy of 80.8%.

3.2. Freshness determination using HSI

TVB-N is the most critical attribute related with freshness. According to the Chinese standard 2707–2016, meat is deemed to be semi-fresh or putrid if the TVB-N is beyond 15 mg/100 g.

As freshness is a complex criterion, generally, more than one attribute are combined to give a comprehensive evaluation of meat. The prediction ability of hyperspectral images within 470–1000 nm for simultaneous determination of TVB-N and pH was explored in Ref. [35]. Meat was classified into three grades: fresh (TVB-N ≤ 15 mg/100 g, pH 5.8–6.0), semi-fresh (TVB-N ≤ 25 mg/100 g, pH 6.0–6.3), and spoiled (TVB-N > 25 mg/100 g, pH > 6.3). Based on a halogen tungsten light source, hyperspectral images were acquired, as shown in **Figure 13a**. The vertical line represented the reflectance information at a certain position on the scanning line, and the horizontal line represented the diffusion information at a certain wavelength. Meat presented different diffusion characteristics at different wavelengths and positions. **Figure 13b** showed the spatial diffusion curves at 635, 760, 575, and 980 nm, and **Figure 13c** showed the reflectance spectra at 0, 5, 10, and 15 mm from the center of the scanning line. It can be seen that the spatial diffusion curve is a symmetrical pattern with a maximum intensity at the center of the scanning line. As the distance from the center increases at both ends, the intensity of the scattered light rapidly decreases. Based on the reflectance spectra pretreated with SG, TVB-N was well predicted with R_p of 0.90. According to the abovementioned classification standard, meat can be discriminated into different grades with total accuracy of 91%.

Another noteworthy report was given in Ref. [36]. The authors designed a portable device based on MSI technology to nondestructively detect TVB-N content in intact meat. The device was composed of hardware system, self-developed programming software, and the built-in prediction model. The schematic map of the developed portable device was shown in **Figure 14**, which mainly included an optical fiber, camera, filter, lens, computer, etc. The working flowchart was as follows: first, place the sample on the bracket, and press the external trigger switch, and then the image acquisition unit triggered the CCD camera to acquire image. Meanwhile, the filters were switched to obtain images at different wavelengths. After image collection, the software performed real-time processing, and the prediction results were displayed real time on the liquid crystal display. The scattering profiles of images were fitted using the four-parameter Lorentzian distribution function, and PLSR model based on the four parameters yielded a satisfactory result with R_p^2 of 0.87 for TVB-N.

Based on the images obtained by a MSI system, GLCM was also explored to extract feature variables for TVB-N prediction. In Ref. [37], features were obtained from three characteristic

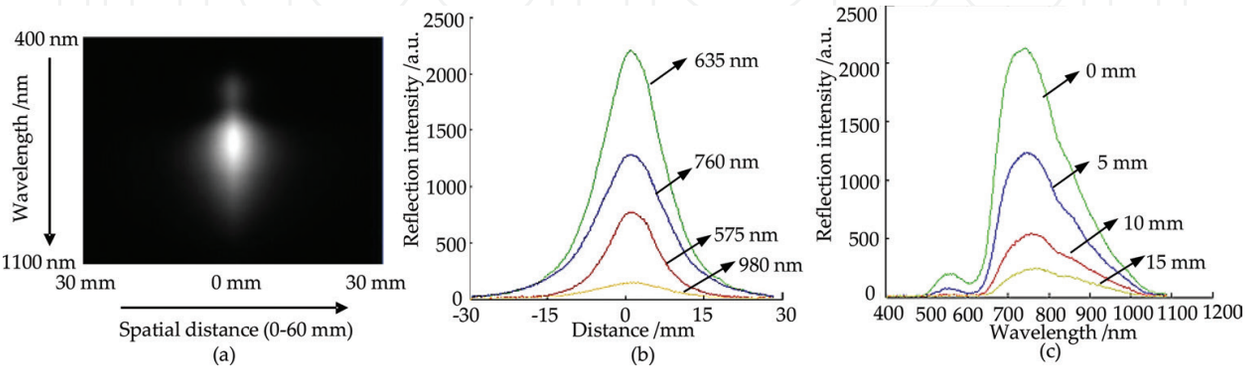

Figure 13. (a) Hyperspectral image of pork, (b) spatial diffusion curves at different wavelengths, and (c) reflectance spectra at different positions.

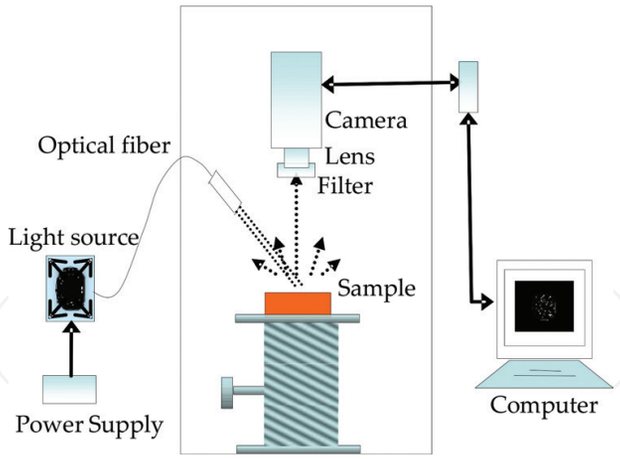

Figure 14. Portable device for TVB-N determination based on MSI.

images at 1280, 1440, and 1660 nm. Then, a new algorithm, namely, back propagation neural network adaptive boosting method, was proposed, obtaining a reasonable prediction result R_p of 0.8325. Their work indicated that the MSI system can be an efficient tool for TVB-N determination, and the research would facilitate its practical usage in meat industry.

4. Conclusions

This chapter summarized the applications of HSI and MSI in quality evaluation and safety control of meat. The current studies have demonstrated the capacity of HSI in quantitatively and qualitatively detection of meat. By integrating both spectroscopic and imaging techniques in one system, the spectral and spatial information of tested samples are acquired simultaneously, which paves way for its extensive applications in meat assessment. As more detailed and comprehensive characteristics of meat are extracted, the quality and safety attributes can be better predicted than using single spectroscopic or imaging technology.

However, despite the fact that the HSI and MSI technology has gained significant development, there are still several drawbacks facing this technology. First, as spectral and spatial information are collected simultaneously, a huge data are acquired for one scanning. Thus, image acquisition and processing become more difficult than other single technologies. With such massive raw image data, it is difficult for HSI systems to be widely implemented for online and real-time application. Secondly, the HSI instrument is relatively expensive compared with conventional methods, thus increasing the cost of commercial detection and impeding its broader adoption. Thirdly, as the nature of nondestructive prediction for HSI technology lies in the establishment of qualitative or quantitative models with reference values, laborious calibration procedures are necessary. Much effort is needed to build accurate models, which makes it time-consuming and costly at the beginning. In addition, the subsequent model updating also requires substantial time, energy, and funds.

To overcome these difficulties, some effort has been taken as possible solutions in response to these disadvantages. On the one hand, to speed up the analysis period, identifying the most

influential wavelengths to eliminate the irrelevant information is an efficient method. In fact, various algorithms for feature wavelengths selection have been proposed for elimination of redundant information and reduction of multicollinearity problem. However, the important variables chosen by different approaches are not consistent even for the same set of spectra, and some selected wavelengths lack of scientific interpretability. Hence, more efficient chemometric methods are in need to improve model performance and robustness. On the other hand, the hardware system with good performance is the precondition and foundation of obtaining stable and high signal-to-noise optical signals. Hence, the enhancement in instrumental development in combination with the availability of high-speed computer will facilitate this technique to be dominant in the future. With further research and development, the HSI and MSI technology can become a powerful tool for online and real-time monitoring the quality and safety of meat.

Acknowledgements

The authors gratefully acknowledge the Special Fund for Agro-scientific Research in the Public Interest Program (Project No. 201003008) and the National Key Research and Development Program (Project No. 2016YFD0401205).

Conflict of interest

We declare that we have no conflict of interest.

Author details

Wenxiu Wang and Yankun Peng*

*Address all correspondence to: ypeng@cau.edu.cn

China Agricultural University, Beijing, China

References

[1] Wojnowski W, Majchrzak T, Dymerski T, Gebicki J, Namiesnik J. Electronic noses: Powerful tools in meat quality assessment. Meat Science. 2017;**131**:119-131. DOI: 10.1016/j.meatsci.2017.04.240

[2] Miller RK. The eating quality of meat. In: Fidel T, editor. Lawrie's Meat Science. 8th ed. Holland: Elsevier; 2017. pp. 461-499. DOI: 10.1016/b978-0-08-100694-8.00015-7

[3] Saucier L. Microbial spoilage, quality and safety within the context of meat sustainability. Meat Science. 2016;**120**:78-84. DOI: 10.1016/j.meatsci.2016.04.027

[4] Peng YK, Dhakal S. Optical methods and techniques for meat quality inspection. Transactions of the Asabe. 2015;**58**:1371-1386. DOI: 10.13031/trans.58.11004

[5] Kamruzzaman M, Barbin D, ElMasry G, Sun DW, Allen P. Potential of hyperspectral imaging and pattern recognition for categorization and authentication of red meat. Innovative Food Science & Emerging Technologies. 2012;**16**:316-325. DOI: 10.1016/j.ifset.2012.07.007

[6] Xiong ZJ, Sun DW, Zeng XA, Xie AG. Recent developments of hyperspectral imaging systems and their applications in detecting quality attributes of red meats: A review. Journal of Food Engineering. 2014;**132**:1-13. DOI: 10.1016/j.jfoodeng.2014.02.004

[7] He HJ, Sun DW. Hyperspectral imaging technology for rapid detection of various microbial contaminants in agricultural and food products. Trends in Food Science & Technology. 2015;**46**:99-109. DOI: 10.1016/j.tifs.2015.08.001

[8] Peng YK, Lu RF. Analysis of spatially resolved hyperspectral scattering images for assessing apple fruit firmness and soluble solids content. Postharvest Biology and Technology. 2008;**48**:52-62. DOI: 10.1016/j.postharvbio.2007.09.019

[9] Kamruzzaman M, Makino Y, Oshita S. Non-invasive analytical technology for the detection of contamination, adulteration, and authenticity of meat, poultry, and fish: A review. Analytica Chimica Acta. 2015;**853**:19-29. DOI: 10.1016/j.aca.2014.08.043

[10] Porep JU, Kammerer DR, Carle R. On-line application of near infrared (NIR) spectroscopy in food production. Trends in Food Science & Technology. 2015;**46**:211-230. DOI: 10.1016/j.tifs.2015.10.002

[11] Peng YK, Lu RF. Prediction of apple fruit firmness and soluble solids content using characteristics of multispectral scattering images. Journal of Food Engineering. 2007;**82**(2):142-152. DOI: 10.1016/j.jfoodeng.2006.12.027

[12] Peng YK. Spectral scattering for assessing quality and safety of meat. In: Lu RF, editor. Light Scattering Technology for Food Property, Quality and Safety Assessment. 1st ed. Boca Raton: CRC Press; 2016. pp. 283-317. DOI: 10.1201/b20220-12

[13] Liu J X, Cao Y, Wang Q, Pan W J, Ma F, et al. Rapid and non-destructive identification of water-injected beef samples using multispectral imaging analysis. Food Chemistry. 2016;**190**:938-943. DOI: http://dx.doi.org/10.1016/j.foodchem.2015.06.056

[14] Wu JH, Peng YK, Li YY, Wang W, Chen JJ, et al. Prediction of beef quality attributes using VIS/NIR hyperspectral scattering imaging technique. Journal of Food Engineering. 2012;**109**:267-273. DOI: 10.1016/j.jfoodeng.2011.10.004

[15] Kamruzzaman M, Makino Y, Oshita S. Online monitoring of red meat color using hyperspectral imaging. Meat Science. 2016;**116**:110-117. DOI: 10.1016/j.meatsci.2016.02.004

[16] Gao XD, Wu JH, Peng YK, Chen JJ, Tao FF. Analysis of beef-marbling grade using hyperspectral imaging technology. Academic Periodical of Farm Products Processing. 2009;**10**:33-37. DOI: 10.3969/j.issn.1671-9646(X).2009.10.008

[17] Huang H, Liu L, Ngadi MO. Prediction of pork fat attributes using NIR images of frozen and thawed pork. Meat Science. 2016;**119**:51-61. DOI: 10.1016/j.meatsci.2016.02.042

[18] Gonzalez-Martin I, Gonzalez-Perez C, Alvarez-Garcia N, Gonzalez-Cabrera JM. On-line determination of fatty acid composition in intramuscular fat of Iberian pork loin by NIRs with a remote reflectance fibre optic probe. Meat Science. 2005;**69**:243-248. DOI: 10.1016/j.meatsci.2004.07.003

[19] Kamruzzaman M, ElMasry G, Sun DW, Allen P. Non-destructive prediction and visualization of chemical composition in lamb meat using NIR hyperspectral imaging and multivariate regression. Innovative Food Science & Emerging Technologies. 2012;**16**:218-226. DOI: 10.1016/j.ifset.2012.06.003

[20] Kobayashi K-I, Matsui Y, Maebuchi Y, Toyota T, Nakauchi S. Near infrared spectroscopy and hyperspectral imaging for prediction and visualisation of fat and fatty acid content in intact raw beef cuts. Journal of Near Infrared Spectroscopy. 2010;**18**(5):301-315. DOI: 10.1255/jnirs.896

[21] Tao FF, Peng YK, Li YY, Chao KL, Dhakal S. Simultaneous determination of tenderness and Escherichia Coli contamination of pork using hyperspectral scattering technique. Meat Science. 2012;**90**:851-857. DOI: 10.1016/j.meatsci.2011.11.028

[22] Tao FF, Peng YK. A method for nondestructive prediction of pork meat quality and safety attributes by hyperspectral imaging technique. Journal of Food Engineering. 2014;**126**:98-106. DOI: 10.1016/j.jfoodeng.2013.11.006

[23] ElMasry G, Sun DW, Allen P. Non-destructive determination of water-holding capacity in fresh beef by using NIR hyperspectral imaging. Food Research International. 2011;**44**:2624-2633. DOI: 10.1016/j.foodres.2011.05.001

[24] Kamruzzaman M, Makino Y, Oshita S. Hyperspectral imaging for real-time monitoring of water holding capacity in red meat. LWT-Food Science and Technology. 2016;**66**:685-691. DOI: 10.1016/j.lwt.2015.11.021

[25] Zhao J, Peng YK. Distribution of beef tenderness grading based on texture feature by hyperspectral image analysis. Transaction of the Chinese Society for Agricultural Machinery. 2015;**31**:279-286. DOI: 10.3969/j.issn.1002-6819.2015.07.039

[26] Tao FF, Peng YK. A nondestructive method for prediction of total viable count in pork meat by hyperspectral scattering imaging. Food and Bioprocess Technology. 2014;**8**(1):17-30. DOI: 10.1007/s11947-014-1374-y

[27] Li HH, Chen QS, Zhao JW, Wu MZ. Nondestructive detection of total volatile basic nitrogen (TVB-N) content in pork meat by integrating hyperspectral imaging and colorimetric sensor combined with a nonlinear data fusion. LWT-Food Science and Technology. 2015;**63**:268-274. DOI: 10.1016/j.lwt.2015.03.052

[28] Tao FF, Wang W, Li YY, Peng YK, Wu JH. A rapid nondestructive measurement method for assessing the total plate count on chilled pork surface. Spectroscopy and Spectral Analysis. 2010;**30**:3405-3409. DOI: 10.3964/ j .issn.1000-0593(2010)12-3405-05

[29] Zhang LL, Peng YK. Noninvasive qualitative and quantitative assessment of spoilage attributes of chilled pork using hyperspectral scattering technique. Applied Spectroscopy. 2016;**70**:1309-1320. DOI: 10.1177/0003702816654060

[30] Peng YK, Zhang J, Wang W, Li YY, Wu JH, Huang H, et al. Potential prediction of the microbial spoilage of beef using spatially resolved hyperspectral scattering profiles. Journal of Food Engineering. 2011;**102**(2):163-169. DOI: 10.1016/j.jfoodeng.2010.08.014

[31] Zheng XC, Peng YK, Wang WX. A nondestructive real-time detection method of total viable count in pork by hyperspectral imaging technique. Applied Sciences. 2017;**7**(3):213. DOI: 10.3390/app7030213

[32] Dissing BS, Papadopoulou OS, Tassou C, Ersbøll BK, Carstensen JM, et al. Using multispectral imaging for spoilage detection of pork meat. Food and Bioprocess Technology. 2012;**6**:2268-2279. DOI: 10.1007/s11947-012-0886-6

[33] Panagou EZ, Papadopoulou O, Carstensen JM, Nychas GJ. Potential of multispectral imaging technology for rapid and non-destructive determination of the microbiological quality of beef filets during aerobic storage. International Journal of Food Microbiology. 2014;**174**:1-11. DOI: 10.1016/j.ijfoodmicro.2013.12.026

[34] Tsakanikas P, Pavlidis D, Panagou E, Nychas GJ. Exploiting multispectral imaging for non-invasive contamination assessment and mapping of meat samples. Talanta. 2016;**161**:606-614. DOI: 10.1016/j.talanta.2016.09.019

[35] Zhang LL, Li YY, Peng YK, Wang W, Jiang FC, et al. Determination of pork freshness attributes by hyperspectral imaging technique. Transactions of the Chinese Society of Agricultural Engineering. 2012;**28**:254-259. DOI: 10.3969/j.issn.1002-6819.2012.07.042

[36] Li CL, Peng YK, Tang XY. Device for rapid nondestructive detection of pork freshness based on multispectral imaging technology. Transactions of the Chinese Society of Agricultural Machinery. 2012;**43**:202-206. DOI: 10.6041/j.issn.1000-1298.2012.S0.040

[37] Huang QP, Chen QS, Li HH, Huang GP, Ouyang Q, Zhao JW. Non-destructively sensing pork's freshness indicator using near infrared multispectral imaging technique. Journal of Food Engineering. 2015;**154**:69-75. DOI: 10.1016/j.jfoodeng.2015.01.006